RSC Advances

ROYAL SOCIETY OF CHEMISTRY

www.rsc.org/advances

Journal Name

RSCPublishing

ARTICLE

Structure resembling effect of clay surface on photochemical properties of *meso*-phenyl or pyridyl-substituted monocationic antimony(V) porphyrin derivatives

Cite this: DOI: 10.1039/xoxxoooooox

Received ooth January 2012,
Accepted ooth January 2012

DOI: 10.1039/xoxxoooooox

www.rsc.org/

T. Tsukamoto,[a, b] T. Shimada[a] and S. Takagi[a]

Four types of *meso*-phenyl or pyridyl-substituted monocationic antimony(V) porphyrin derivatives (Sb^{V}Pors)—5,10,15,20-tetraphenyl; 5,10,15-triphenyl-20-mono(4-pyridyl); 5,15-diphenyl-10,20-di(4-pyridyl); and 5,10,15,20-tetra(4-pyridyl)porphyrinato dihydroxo antimony(V) chloride—with different hydrophobicities were synthesised, and their photochemical properties on anionic clay were investigated. The absorption and fluorescence behaviour of the Sb^{V}Pors were strongly affected by complex formation with clay. Interestingly, the absorption transition probabilities and fluorescence quantum yields of the Sb^{V}Pors prominently increased on the clay surface. The more hydrophobic Sb^{V}Por showed greater absorption transition probability increase and fluorescence quantum yield enhancement. These unique effects of the highly flat clay surface on the photochemical behaviour of Sb^{V}Por were discussed mainly from the viewpoint of transition probability, by using the potential energy curves of Sb^{V}Por with and without clay. For the more hydrophobic Sb^{V}Por, the molecular structure of the ground and excited states on the clay surface tended to become similar because of the strong hydrophobic interaction between porphyrin and the clay surface, i.e. the 'structure resembling effect'. This effect induces a change in the transition probabilities.

Introduction

The photochemical behaviour of dye molecules on or in inorganic host materials such as silica[1-4], zeolite[1,5] and nanosheet[1,6-28] materials have been investigated by many researchers. The unique effects of complex formation with inorganic materials on the photochemical properties of dyes, such as increase in the absorption coefficient[29] and enhancement of fluorescence intensity,[29,30] have been reported. The aforementioned valuable effects of nanosheet materials can be exploited for developing photochemical reaction systems and photofunctional materials. However, the mechanism underlying these effects has not been clarified in detail; in addition, dye molecules easily form aggregates on inorganic surfaces, which may decrease their excited lifetimes[31] and result in low photoactivity. Thus, we believe that clarification of the mechanism of such effects and control of the assembly structure of dye molecules on inorganic surfaces are important subjects in photochemical materials chemistry. Recently, we have succeeded in suppressing the aggregation of dyes on an inorganic surface even under high-density conditions by using the 'size-matching effect' or 'intercharge distance matching effect'.[28,32] In a typical case, the effect can be realised by using negatively charged clay minerals. This effect is rationalised by matching the distances between the cationic sites in the dye molecule and the anionic sites on the clay surface. Under the conditions this effect is active, the photochemical behaviour of dyes on the inorganic surface can be tuned without any problems caused by aggregation. This effect enables us to examine the influence of the inorganic surface on the photochemical properties of dyes in a straightforward manner.

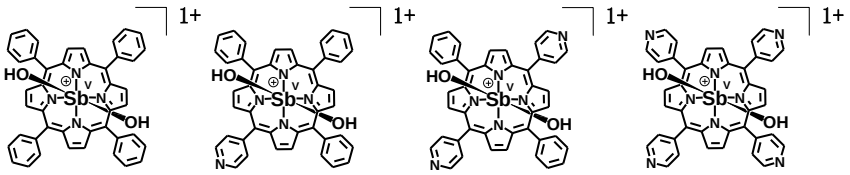

$[Sb^{V}(TPP)(OH)_2]^{1+}$ $[Sb^{V}(MPyP)(OH)_2]^{1+}$ $[Sb^{V}(DPyP)(OH)_2]^{1+}$ $[Sb^{V}(TPyP)(OH)_2]^{1+}$

Figure 1. Structures of dihydroxo(5,10,15,20-tetraphenylporphyrinato)antimony(V) chloride ($[Sb^{V}(TPP)(OH)_2]Cl$), dihydroxo[5,10,15-triphenyl-20-mono(4-pyridyl)-porphyrinato]antimony(V) chloride ($[Sb^{V}(MPyP)(OH)_2]Cl$), dihydroxo[5,15-diphenyl-10,20-di(4-pyridyl)porphyrinato]antimony(V) chloride ($[Sb^{V}(DPyP)(OH)_2]Cl$) and dihydroxo[5,10,15,20-tetra(4-pyridyl)porphyrinato]antimony(V) chloride ($[Sb^{V}(TPyP)(OH)_2]Cl$).

Clay minerals are interesting multilayered inorganic host materials for organic-inorganic complexes.[1,6-10,27,28,33] Clay minerals such as saponite have cation exchange capacity (CEC) because of its negatively charged structure. The stoichiometric formula of saponite used in this study is $[(Si_{7.2}Al_{0.8})(Mg_{5.97}Al_{0.03})O_{20}(OH)_4]^{-0.77}(Na_{0.49}Mg_{0.14})^{+0.77}$. The theoretical surface area is 750 m^2 g^{-1} and the CEC is 99.7 mequiv / 100 g.[11] The structure of synthetic saponite is shown in Figure S1 in the Electronic supplementary information (ESI†). While the nanosheet stacks in the solid state, it swells easily and completely exfoliates into a single sheet in aqueous solution under sufficient dilution. Since the aqueous solution of saponite is transparent in the UV-visible range when the exfoliated particle size in water is small (< ~100 nm), it is suitable for optical measurement.

Upon complex formation with clay, the absorption maxima of porphyrin are shifted to longer wavelength because of the flattening of the *meso*-substituent with respect to the plane of the porphyrin ring[11,19,23]. Fluorescence enhancement and increased excited lifetime have been observed for some dye molecules upon complex formation with clay[29,30,34,35], probably because of the suppression of non-radiative deactivation. The adsorption pattern of dyes onto the clay surface, such as electrostatic and hydrophobic interactions, would relate to such photochemical effects of the clay surface. To clarify the mechanism for such changes in the photochemical properties, we recently reported the photochemical behaviour of mono-, tri- and pentacationic antimony(V) porphyrin derivatives, wherein electrostatic and hydrophobic interactions with clay were modulated systematically[29]. For these molecules, the radiative deactivation rate constants on the clay surface, denoted as k_f^C, were much different from those without clay in water, k_f^W. The effect of the clay surface can be expressed in terms of k_f^C / k_f^W values for changes in the deactivation rate constants. The less cationic antimony porphyrins showed an increasing trend in k_f^C / k_f^W. Attempts have been made to rationalise this trend on the basis of changes in the transition probability by using potential energy curves of the ground and excited states of the dye molecule. Two observations have been reported: (i) the most stable structures become relatively similar between the ground and excited states (structure resembling effect, SRE), leading to an increase in k_f; (ii) the potential energy curves are relatively sensitive to nuclear coordinates (structure fixing effect, SFE), leading to a decrease in k_f. We have proposed that changes in the k_f^C/k_f^W values are determined by a balance between the SRE and the SFE[29,30]. This balance would be determined by the adsorption pattern, i.e. hydrophobic and electrostatic interactions between the dye molecules and the clay surface. In the case of previously examined mono-, tri- and pentacationic antimony(V) porphyrin, both hydrophobic and electrostatic interactions between the dye and the clay surface were modulated; hence, it was difficult to distinguish between the effects of these interactions.

For this reason, in the present study, we have investigated antimony(V) porphyrin derivatives (Sb^{V}Pors) having the same charge number (+1) but different hydrophobicity. The use of such dyes might aid in clarifying the importance of the hydrophobic and electrostatic interactions between the dye and the clay. The designed Sb^{V}Pors are 5,10,15,20-tetraphenyl, 5,10,15-triphenyl-20-mono(4-pyridyl), 5,15-diphenyl-10,20-di(4-pyridyl) and 5,10,15,20-tetra(4-pyridyl)porphyrinato dihydroxo antimony(V) chloride; these are denoted as $[Sb^{V}(TPP)(OH)_2]Cl$, $[Sb^{V}(MPyP)(OH)_2]Cl$, $[Sb^{V}(DPyP)(OH)_2]Cl$ and $[Sb^{V}(TPyP)(OH)_2]Cl$, respectively (Figure 1). The Sb^{V}Pors are monocationic porphyrins[24,36-42] and adsorb on the clay surface via hydrophobic and electrostatic interactions[24-26,29]. The hydrophobicity of the Sb^{V}Pors is controlled by changing the number of *meso*-phenyl and pyridyl substituents, under the same charge number in the molecule. Sb^{V}TPP having four *meso*-phenyl substituents is readily soluble in chloroform and poorly soluble in water. Its saturated solubility in water is 1×10^{-4} M. On the other hand, Sb^{V}TPyP having four *meso*-pyridyl substituents is readily soluble in water and insoluble in chloroform. The adsorption behaviour and photochemical properties of these cationic Sb^{V}Pors on the anionic clay surface were investigated by UV-visible absorption, as well as steady and time-resolved fluorescence spectroscopy. The complexes were examined in water, in which the saponite clay sheet is exfoliated as a single nanosheet.

Results and Discussion

Absorption behaviours of Sb^{V}Pors with and without clay

The aqueous clay dispersion was essentially transparent in the UV-visible region under the present experimental conditions. UV-visible absorption spectra of the porphyrins in water and those adsorbed on the saponite surface were recorded. The absorption spectra of all Sb^{V}Por with and without clay are shown in Figure 2.

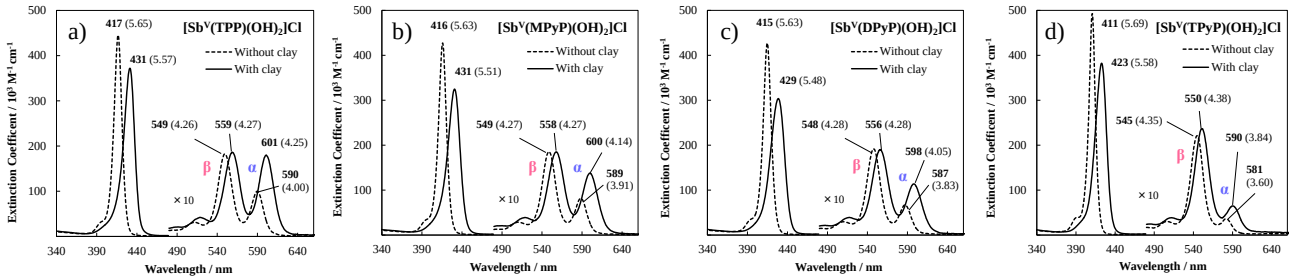

Figure 2. Absorption spectra of a) Sb^{V}TPP, b) Sb^{V}MPyP, c) Sb^{V}DPyP and d) Sb^{V}TPyP with and without clay in water. Absorption maxima (λ_{max} / nm) and extinction coefficients (log ε_{max}) are shown. [Sb^{V}Por] = 6.0 × 10^{-6} M. [clay] = 6.0 × 10^{-5} equiv L^{-1} and the loading levels of porphyrins are 10% versus CEC of the clay. The lower-energy band of the Q-band is denoted as α (0,0) and the higher-energy band is denoted as β (1,0).

All porphyrins exhibited a spectral shift to longer wavelengths upon complex formation with clay. Aggregation species that induce the spectral shift were not observed at 10% loading versus CEC of the clay, judging from the experiment involving changes in the loading level (not shown). These redshifts of the porphyrin upon adsorption on the clay surface are mainly induced by co-planarisation of the *meso*-substituents with respect to the porphyrin rings[11,19,23]. Co-planarisation of the adsorbed molecule is induced by the highly flat surface of the clay, when the molecules adsorb on the surface in a parallel fashion. Thus, the degree of redshift is useful to discuss the adsorption conditions of molecules on the clay surface, such as the degree of molecular flattening. The spectral shifts ($\Delta\lambda_{max}$) at the longest Q-band wavelength were 11 nm (0.039 eV) for Sb^{V}TPP, Sb^{V}MPyP and Sb^{V}DPyP and 9 nm (0.033 eV) for Sb^{V}TPyP at 10% vs. CEC of the clay. There were almost no differences between the $\Delta\lambda_{max}$ values of the Sb^{V}Pors. This result suggested that the structures of the Sb^{V}Pors adsorbed on the clay surface are flattened compared to those in bulk solution and that their molecular structures and adsorption orientations with respect to the clay surface are similar.

Interestingly, the values of the oscillator strength (f^{C}) estimated from the integrals of the extinction coefficients ($\int\varepsilon d\bar{\nu}$ / M^{-1} cm^{-2}) in the Q-band wavenumber range on the clay surface were distinctly different, while those in the bulk solution (f^{W}) were almost the same (Table 1), according to eq 1 [43].

$$f = 4.3 \times 10^{-9} \int \varepsilon d\bar{\nu} \qquad (1)$$

For all porphyrins, the f^{C} values increased by 1.34–1.41 times over the f^{W} values. The increase in the transition probability of the porphyrin would be due to the increased Franck-Condon factor[43] on the clay surface, as will be described later.

It should be noted that the Q-band shapes of the Sb^{V}Pors with and without clay are different. The lower-energy band of the Q-bands is denoted as α (0,0) and the higher-energy band is denoted as β (1,0). The ratios of the extinction coefficients of the α (0,0) and β (1,0) bands (ε_α / ε_β) with and without clay are summarised in Table 1. The ε_α / ε_β values on the clay surface increased by 1.62–1.74 times as compared to those in the bulk solution. These results indicate that the transition probabilities of the α (0,0) and β (1,0) bands changed, because of the change in each Franck-Condon factor. The increase in the extinction coefficients and ε_α / ε_β values strongly suggests that the molecular structures of the ground and excited states of porphyrin become similar via the complex formation with the clay (SRE, described later). The increases in the f and ε_α / ε_β values tend to be more pronounced for the more hydrophobic Sb^{V}Por. This tendency indicates that highly hydrophobic Sb^{V}Pors are influenced more strongly by the SRE. Additionally, the plot of $(\varepsilon_\alpha / \varepsilon_\beta)^{C}$ / $(\varepsilon_\alpha / \varepsilon_\beta)^{W}$ against f^{C} / f^{W} for the Sb^{V}Pors is linear (Figure S2, ESI†). It is suggested that the increases in the f and ε_α / ε_β values are caused by a common factor. The details will be described in the discussion section.

Fluorescence behaviour of Sb^{V}Pors with and without clay

Fluorescence spectra of the porphyrins in water and those adsorbed on the clay surface were observed. The fluorescence spectra of the porphyrins with and without clay are shown in Figure 3. The loading levels of the Sb^{V}Pors were set at 2.0% versus CEC, where aggregation was not observed.

Table 1. Integrals of Oscillator Strengths (f) in the Q-band Wavenumber Range and Ratios (ε_α / ε_β) of Extinction Coefficients of α (0,0) and β (1,0) bands of Sb^{V}Pors with and without Clay in Water

Compound	Oscillator strength			Ratio of extinction coefficients of α and β-bands		
	f^{W}	f^{C}	f^{C} / f^{W}	$(\varepsilon_\alpha / \varepsilon_\beta)^{W}$	$(\varepsilon_\alpha / \varepsilon_\beta)^{C}$	$(\varepsilon_\alpha / \varepsilon_\beta)^{C}$ / $(\varepsilon_\alpha / \varepsilon_\beta)^{W}$
[Sb^{V}(TPP)(OH)$_2$]Cl	0.102	0.144	1.41	0.550	0.955	1.74
[Sb^{V}(MPyP)(OH)$_2$]Cl	0.0959	0.133	1.39	0.437	0.741	1.70
[Sb^{V}(DPyP)(OH)$_2$]Cl	0.0950	0.129	1.36	0.355	0.589	1.66
[Sb^{V}(TPyP)(OH)$_2$]Cl	0.0955	0.128	1.34	0.178	0.288	1.62

The integral range is 14500 to 20400 cm^{-1} (490 to 690 nm). f^{W} and f^{C} are the f values of Sb^{V}Por without and with clay. ε_α and ε_β are extinction coefficients of the α (0,0) and β (1,0) bands. $(\varepsilon_\alpha / \varepsilon_\beta)^{W}$ and $(\varepsilon_\alpha / \varepsilon_\beta)^{C}$ are the $\varepsilon_\alpha / \varepsilon_\beta$ of Sb^{V}Por without and with clay.

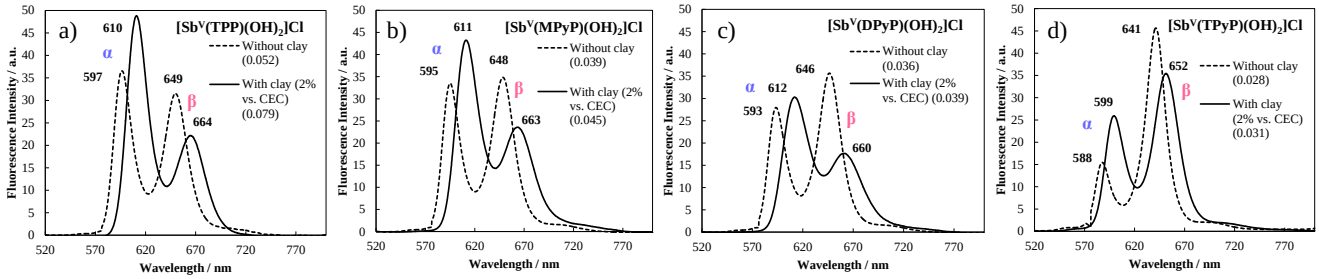

Figure 3. Fluorescence spectra and fluorescence peaks (λ_{em} / nm) excited at 430 and 417 nm, 430 and 416 nm, 430 and 415 nm and 420 and 410 nm for a) Sb^{V}TPP, b) Sb^{V}MPyP, c) Sb^{V}DPyP and d) Sb^{V}TPyP with and without clay in water, respectively. The fluorescence quantum yields (Φ_f) are shown in parentheses. The higher-energy band is denoted as α (0,0) and the lower-energy band is denoted as β (0,1). [Sb^{V}Por] = 1.0×10^{-7} M. [clay] = 5.0×10^{-6} equiv L^{-1}. (The loading levels of porphyrins are 2.0% versus CEC of the clay).

In all of the porphyrins, redshift of the fluorescence maxima (λ_{em}) was observed upon complex formation with the clay. In addition, the shapes of the fluorescence spectra, i.e. the ratio of the α (0,0) and β (0,1) band intensities (i_α / i_β) were altered, as shown in Table 2. The increase in the i_α / i_β values tended to be more effective for the more hydrophobic Sb^{V}Por. The fluorescence quantum yields (Φ_f) are summarised in Table 3. Φ_f^W and Φ_f^C are the Φ_f values for Sb^{V}Por without clay and with clay, respectively. The Φ_f values for the Sb^{V}Pors tended to increase upon complex formation with the clay, as compared to those without clay. For the more hydrophobic Sb^{V}Por, the Φ^C / Φ^W values seemed to increase.

To discuss the photochemical behaviour of the porphyrins on the clay surface in detail, time-resolved fluorescence spectra for each porphyrin with and without clay were measured and the excited lifetime was determined by using a picosecond fluorescence measurement system. The loading levels of the Sb^{V}Pors were set at 0.05% versus CEC. As shown in Figure 4, all the decay curves for the porphyrins with and without clay could be analysed as a single exponential decay, and the fluorescence lifetimes (τ) were obtained. Such simple fluorescence decay is rarely observed for dyes on an inorganic surface. In this experiment, suppression of dye aggregation simplifies the photochemical behaviour. The value of τ^W, τ^C and τ^C / τ^W are summarised in Table 3. The values of τ^C / τ^W are almost the same for all the Sb^{V}Pors except for Sb^{V}TPyP.

The radiative deactivation rate constants (k_f) were calculated by using the Φ_f and τ values according to eq 2, and are shown in Table 3. The ratios of k_f^C and k_f^W are also shown in Table 3 to discuss the effects of clay in detail.

$$k_f = \Phi_f/\tau \qquad (2)$$

Table 2. Ratios of Fluorescence Intensities of the α (0,0) and β (0,1) bands of Sb^{V}Por with and without Clay in Water

Compound	Ratio of fluorescence intensities of α and β-bands		
	$(i_\alpha / i_\beta)^W$	$(i_\alpha / i_\beta)^C$	$(i_\alpha / i_\beta)^C / (i_\alpha / i_\beta)^W$
[Sb^V(TPP)(OH)$_2$]Cl	1.16	2.20	1.89
[Sb^V(MPyP)(OH)$_2$]Cl	0.961	1.83	1.91
[Sb^V(DPyP)(OH)$_2$]Cl	0.784	1.72	2.19
[Sb^V(TPyP)(OH)$_2$]Cl	0.338	0.733	2.16

i_α and i_β are fluorescence intensities of α (0,0) and β (0,1) bands. (i_α / i_β)^W and (i_α / i_β)^C are the i_α / i_β values of Sb^{V}Por without and with clay.

Discussion of photochemical properties of Sb^{V}Pors with and without clay

Theory of SRE and SFE using potential energy curves of ground and excited states. Attempts have been made to discuss the effects of complex formation with clay on the photochemical properties of dyes by using the potential energy curves of the ground and excited states of the dye molecule[29,30]. The potential energy curve of the excited state would be broader than that of the ground state because the force constant in the excited state is relatively small[44]. In this study, the sharpness of the two energy curves are assumed to be comparable. At least two types of effects might result from complex formation with a clay: (i) the most stable structure becomes more similar for the ground and excited states (SRE) and (ii) the potential energy curves become relatively sensitive to nuclear coordinates (SFE) (Figure 5, i and ii)[29,30].

The SRE induces an increase in the Franck-Condon factor $(\int \chi_0 \chi'_0 dr)^2$ for the S_0-S_1 electronic transition and radiative deactivation for the wavefunction overlap of v_0-v'_0. This effect should lead to an increase in the f, ε_α / ε_β, k_f and i_α / i_β values. f and k_f are theoretically proportional to $(\int \chi_0 \chi'_0 dr)^2$ [43]. On the other hand, assuming that the two energy curves are influenced by the same sharpness effect of the clay, the SFE induces a decrease in $(\int \chi_0 \chi'_0 dr)^2$, leading to a decrease in k_f.

Based on these effects, the present result is discussed in the

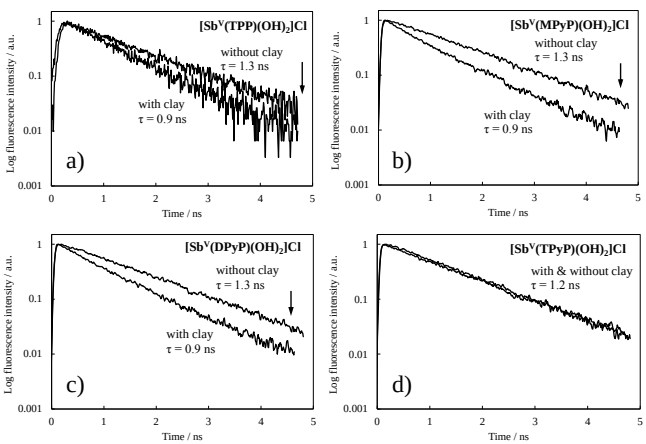

Figure 4. Fluorescence decay profile and fluorescence lifetimes (τ) for a) Sb^{V}TPP, b) Sb^{V}MPyP, c) Sb^{V}DPyP and d) Sb^{V}TPyP with and without clay in water. The decay profile and fluorescence lifetime for Sb^{V}TPP are adapted from our previous report[29]. [Sb^{V}Por] = 2.0×10^{-8} M. [clay] = 4.0×10^{-5} equiv L^{-1}. The porphyrin loadings on the clay surface are 0.05% vs. CEC.

Table 3. Fluorescence Quantum Yields (Φ_f), Fluorescence Lifetimes (τ), and Radiative Deactivation Rate Constants (k_f) of Sb^{V}Por with and without Clay in Water

Compound	Fluorescence quantum yield			Fluorescence lifetime / 10^{-9} s			Radiative deactivation rate constant / 10^{9} s^{-1}		
	Φ_f^W	Φ_f^C	Φ_f^C / Φ_f^W	τ^W	τ^C	τ^C / τ^W	k_f^W	k_f^C	k_f^C / k_f^W
$[Sb^{V}(TPP)(OH)_2]Cl$[a]	0.052	0.079	1.52	1.3	0.9	0.7	0.040	0.087	2.2
$[Sb^{V}(MPyP)(OH)_2]Cl$	0.037	0.043	1.16	1.3	0.9	0.7	0.029	0.048	1.7
$[Sb^{V}(DPyP)(OH)_2]Cl$	0.035	0.038	1.09	1.3	0.9	0.7	0.027	0.042	1.6
$[Sb^{V}(TPyP)(OH)_2]Cl$	0.027	0.030	1.10	1.2	1.2	1.0	0.022	0.025	1.1

Φ_f^W and Φ_f^C are the Φ_f values of Sb^{V}Por without and with clay. The Φ_f values are fluorescence quantum yields excited at 417 and 430 nm, 416 and 430 nm, 415 and 430 nm, and 410 and 420 nm for Sb^{V}TPP, Sb^{V}MPyP, Sb^{V}DPyP, and Sb^{V}TPyP without and with clay, respectively. τ^W and τ^C are the τ values of Sb^{V}Por without and with clay. The τ values are fluorescence lifetimes excited at 415 and 430 nm, 415 and 430 nm, 415 and 430 nm, and 410 and 430 nm for Sb^{V}TPP, Sb^{V}MPyP, Sb^{V}DPyP and Sb^{V}TPyP without and with clay, respectively. k_f^W and k_f^C are the k_f values of Sb^{V}Por without and with clay. a: Adapted from our previous report[29].

next section. The major interactions between the Sb^{V}Por molecules and the clay surface would be hydrophobic and electrostatic.

Effect of complex formation with clay on the photochemical behaviour of Sb^{V}Pors. The photochemical properties of the Sb^{V}Pors changed upon complex formation with clay. The f and ε_α / ε_β values increased because of adsorption onto the clay for all the Sb^{V}Pors (Table 1). The increased f values indicate that the electronic transition probabilities from the S_0 to S_1 states of the Sb^{V}Pors on the clay surface increase as compared with those in the bulk aqueous solution. The increased ε_α / ε_β values suggest that the Franck-Condon factors $(\int\chi_0\chi'_0 dr)^2$ for the v_0-v'_0 transitions of the Sb^{V}Pors increase because of adsorption onto the clay. These results clearly indicate that the changes in the electronic transition probabilities of the Sb^{V}Pors on clay are attributed to changes in the Franck-Condon factors, as the potential curves of the ground and excited states resemble each other; i.e. the SRE. These considerations are also indicated by the fact that the k_f and i_α / i_β values of Sb^{V}Por increased on the clay surface as compared with those in the bulk aqueous solution, judging from the fluorescence and absorption spectra of all Sb^{V}Pors (Tables 2, 3).

Additionally, there were differences in the photochemical changes on clay between the four types of Sb^{V}Pors. The f^C / f^W and $(\varepsilon_\alpha$ / $\varepsilon_\beta)^C$ / $(\varepsilon_\alpha$ / $\varepsilon_\beta)^W$ values for the more hydrophobic Sb^{V}Pors were larger than those for the more hydrophilic ones according to the absorption spectra (Table 1 and Figure S2, ESI†). These facts indicate that the SRE is stronger for the more hydrophobic Sb^{V}Pors. It is also suggested that the changes in these photochemical parameters are caused only by the SRE and not the SFE, which decreases the transition probabilities. The linear relationship between the f^C / f^W values and the $(\varepsilon_\alpha$ / $\varepsilon_\beta)^C$ / $(\varepsilon_\alpha$ / $\varepsilon_\beta)^W$ values also supports this interpretation (Figure S2, ESI†). Moreover, in the case of fluorescence, the k_f^C / k_f^W values showed similar trends as above (Table 3). On the other hand, the i_α / i_β values did not depend on the hydrophobicity of Sb^{V}Por. The absorption properties should directly reflect the molecular potential curves, as opposed to the fluorescence properties. The fluorescence properties may include differences in the nuclear configuration induced by solvent relaxation for the excited Sb^{V}Pors, because of the difference in molecular symmetry. The adsorption behaviour of Sb^{V}Pors on the clay surface are influenced by the hydrophobic and electrostatic interactions between the dye molecules and the clay. In this study, only the effect originated from the hydrophobic interactions is discussed strictly because all characteristics of the Sb^{V}Pors, such as cation charge, molecular structure and type of counter anion are identical except for hydrophobicity. Therefore, it is apparent that the hydrophobic interaction between the Sb^{V}Pors and the clay is more effective; consequently, the SRE is dominant.

To conclude, it is clear that hydrophobic interactions between the Sb^{V}Pors and the clay are affected mainly by the SRE and that the contribution of the SFE is small. The hydrophobic interactions originate from a solvent iceberg formed by a hydrogen bonding network on the hydrophobic molecular surfaces. The areas where the hydrophobic interaction is active vary between the Sb^{V}Pors because the solvent iceberg is expected to be formed on the hydrophobic

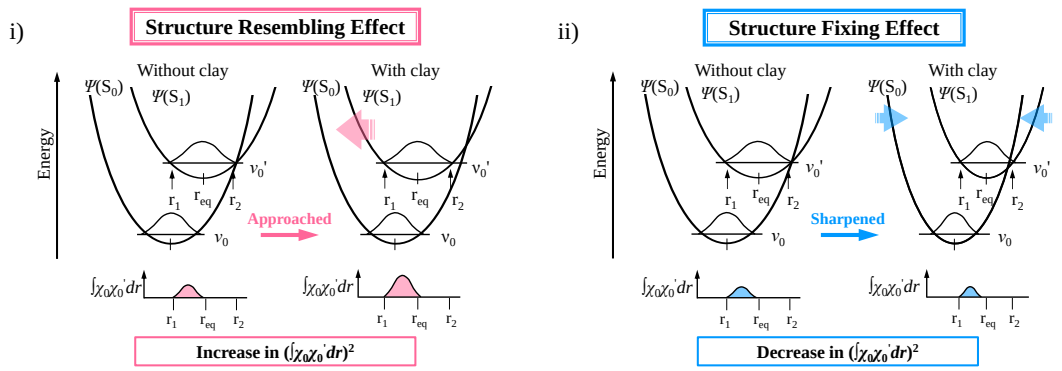

Figure 5. Plausible conceptual potential energy curves of the ground and excited states of 1+ charged Sb^{V}Pors without and with clay. i) Structure resembling effect (SRE) between the ground and excited states and ii) structure fixing effect (SFE) on the clay surface are shown. $(\int\chi_0\chi'_0 dr)^2$ is the Franck-Condon factor for the wavefunction overlap of v_0-v'_0. In the SFE, it is assumed that the two energy curves of the ground and excited states are influenced by the same sharpness effect of clay. v_0 and v'_0 denote the lowest vibration states in the ground and excited states, respectively.

porphyrin and *meso*-phenyl planar aromatic rings, but not on the hydrophilic *meso*-pyridyl. Therefore, the hydrophobic interaction is larger for the Sb^{V}Por having a greater number of *meso*-phenyl substituents and smaller for that having a greater number of *meso*-pyridyl ones. This interaction is expected to fix the porphyrin molecules in the longitudinal direction against the flat clay surface. Considering parallel adsorption of planar porphyrin molecules on the clay, the entire guest molecular structure may be fixed. On the other hand, electrostatic interactions originate from Coulomb's forces between the cation site of the guest molecule and the anion point of the clay. The electrostatic interaction is the same for all the Sb^{V}Pors because of the similar cation charge. When using a guest molecule having multiple cations, this interaction is expected to fix the molecules not only in the longitudinal direction but also in the transverse direction against the clay surface, because there are multiple fixed points in the molecular structure. In this study, since monocationic porphyrins are used, the SRE originating from the hydrophobic interactions between porphyrin and the clay surface play an important role.

Experimental

Materials and method

Clay minerals (saponite): Sumecton SA was received from Kunimine Industries Co., Ltd. Dihydroxo(5,10,15,20-tetraphenylporphyrinato)antimony(V) chloride ($[Sb^{V}(TPP)(OH)_2]Cl$, denoted as Sb^{V}TPP), dihydroxo[5,10,15-triphenyl-20-mono(4-pyridyl)porphyrinato]antimony(V) chloride ($[Sb^{V}(MPyP)(OH)_2]Cl$, denoted as Sb^{V}MPyP), dihydroxo[5,15-diphenyl-10,20-di(4-pyridyl)porphyrinato]antimony(V) chloride ($[Sb^{V}(DPyP)(OH)_2]Cl$, denoted as Sb^{V}DPyP) and dihydroxo[5,10,15,20-tetra(4-pyridyl)porphyrinato]antimony(V) chloride ($[Sb^{V}(TPyP)(OH)_2]Cl$, denoted as Sb^{V}TPyP) were synthesised following the procedure described in the Supplementary Information.

UV-visible absorption spectra were measured on a Shimadzu UV-3150 spectrophotometer. Emission spectra were recorded on a Jasco FP-6600 spectrofluorometer.

Time-resolved fluorescence signals were measured using a Hamamatsu Photonics C4780 system based on a streak detector. A Nd^{3+} YAG laser with an optical parametric generator (EKSPLA PL2210JE + PG-432, FWHM 25 ps, 1 kHz) was used for excitation.

Sample preparation

For measurement of absorption spectra: Exfoliated porphyrin/saponite complexes were prepared by mixing aqueous clay dispersions and the respective cationic porphyrin aqueous solutions under stirring. The porphyrin loadings were set at 10% vs. CEC.

For measurement of fluorescence spectra: The porphyrin/saponite complexes were prepared using the same method as that in the case of absorption spectral measurement. The porphyrin loadings were set at 2% vs. CEC. The fluorescence quantum yields of porphyrins were determined using $[H_2TMPyP]Cl_4$ as the standard ($\Phi_f = 0.050$) [45].

For measurement of time-resolved fluorescence spectra: The porphyrin/saponite complexes were prepared using the same method as that in the case of absorption spectral measurement. The porphyrin loadings were set at 0.05% vs. CEC.

Conclusions

Four types of *meso*-phenyl or pyridyl substituted mono-cationic antimony(V) porphyrin derivatives (Sb^{V}Pors) having different hydrophobicity were synthesised, and their photochemical properties on anionic clay were investigated. The absorption spectra of Sb^{V}Por/clay complexes shifted to the longer wavelength region because of the flattening of the molecules on the clay surface. The extinction coefficients and radiative deactivation rate constants of Sb^{V}Pors on the clay surface increased notably compared to those in the bulk aqueous solution. This result indicates that electronic transition probabilities of Sb^{V}Pors between the S_0 and S_1 states increased. Moreover, the absorbance ratios of the v_0-v'_0 to v_0-v'_1 transitions and the fluorescence ratios of the v'_0-v_0 to v'_0-v_1 transitions of Sb^{V}Pors on the clay surface were higher compared to those in the bulk aqueous solution. Therefore, it is suggested that the electronic transition probability would increase because of the increase in the Franck-Condon factor due to the increased overlap of vibrational wave functions between the S_0 and S_1 states. These considerations are rationalised by the resemblance of the molecular structures of the ground and excited states (SRE). Interestingly, the increase in the photochemical parameters of Sb^{V}Pors on clay was more prominent for the more hydrophobic Sb^{V}Pors. Cationic dyes adsorb on anionic clay through hydrophobic and electrostatic interactions. In this case, only the difference in hydrophobic interactions can be considered because Sb^{V}Pors having the same cation charge have identical electrostatic interaction strength. Thus, it is suggested, for the first time, that the hydrophobic interaction between dyes and clay primarily effects the SRE. These findings are beneficial for the development of efficient photochemical reaction systems using dye-clay complexes.

Acknowledgements

This work has been partly supported by a Grant-in-Aid for Scientific Research (B), Grant-in-Aid for Scientific Research on Innovative Areas (No. 25107521) and Grant-in-Aid for JSPS Research Fellows (No. 263441).

Notes and references

[a] Department of Applied Chemistry, Graduate Course of Urban Environmental Sciences, Tokyo Metropolitan University, Minami-ohsawa 1-1, Hachiohji, Tokyo 192-0397 Japan Tel.: +81 42 677 2839; fax: +81 42 677 2838

[b] Japan Society for the Promotion of Science (JSPS / DC2), Ichibancho, Chiyoda-ku, Tokyo 102-8471 Japan

† Electronic Supplementary Information (ESI) available: The structure of synthetic saponite (Figure S1, ESI), the plot of $(\varepsilon_\alpha / \varepsilon_\beta)^C / (\varepsilon_\alpha / \varepsilon_\beta)^W$ vs. f^C / f^W for Sb^{V}Pors (Figure S2, ESI), and the section entitled "The synthesis of Sb^{V}Pors" are available. See DOI: 10.1039/b000000x/

1 J. K. Thomas, *Chem. Rev.*, 1993, **93**, 301-320.

2 T. Yui, Y. Kobayashi, Y. Yamada, K. Yano, Y. Fukushima, T. Torimoto, K. Takagi, *ACS Appl. Mater. Interfaces*, 2011, **3**, 931-935.

3 S. Inagaki, O. Ohtani, Y. Goto, K. Okamoto, M. Ikai, K. Yamanaka, T. Tani, T. Okada, *Angew. Chem. Ind. Ed*., 2009, **48**, 4042-4046.
4 K. Fujii, N. Iyi, H. Hashizume, S. Shimomura, T. Ando, *Chem. Mater*., 2009, **21**, 1179-1181.
5 K. J. Thomas, R. B. Sunoj, J. Chandrasekhar, V. Ramamurthy, *Langmuir*, 2000, **16**, 4912-4921.
6 K. Takagi, T. Shichi, *J. Photochem. Photobiol. C: Photochem. Rev.*, 2000, **1**, 113-130.
7 F. Lopez Arbeloa, V. Martinez, T. Arbeloa, I. Lopez Arbeloa, *J. Photochem. Photobiol. C: Photochem. Rev.*, 2007, **8**, 85-108.
8 J. Bujdak, *Appl. Clay Sci.*, 2006, **34**, 58-73.
9 R. Ras, Y. Umemura, C. Johnston, A. Yamagishi, R. Schoonheydt, *Phys. Chem. Chem. Phys*., 2007, **9**, 918-932.
10 H. Sato, Y. Hiroe, K. Tamura, A. Yamagishi, *J. Phys. Chem. B*, 2005, **109**, 18935-18941.
11 S. Takagi, T. Shimada, M. Eguchi, T. Yui, H. Yoshida, D. A. Tryk, H. Inoue, *Langmuir*, 2002, **18**, 2265-2272.
12 J. Bujdak, P. Komadel, *J. Phys. Chem. B*, 1997, **101**, 9065-9068.
13 J. Bujdak, N. Iyi, *Clays Clay Minerals*, 2002, **50**, 446-454.
14 G. K. Pushpito, A. Bard, *J. Phys. Chem.*, 1984, **88**, 5519-5526.
15 Z. Grauer, D. Avnir, S. Yariv, *Can. J. Chem.*, 1984, **62**, 1889-1894.
16 N. Miyamoto, R. Kawai, K. Kuroda, M. Ogawa, *Applied Clay Sci.*, 2000, **16**, 161-170.
17 N. Iyi, R. Sasai, T. Fujita, T. Deguchi, T. Sota, F. Lopez Arbeloa, K. Kitamura, *Applied Clay Sci.*, 2002, **22**, 125-136.
18 M. Ogawa, K. Kuroda, *Chem. Rev.*, 1995, **95**, 399-438.
19 Z. Chernia, D. Gill, *Langmuir*, 1999, **15**, 1625-1633.
20 V. G. Kuykendall, J. K. Thomas, *Langmuir*, 1990, **6**, 1350-1356.
21 D. R. Kosiur, *Clays Clay Minerals*, 1977, **25**, 365-371.
22 S. S. Cady, T. J. Pinnavaia, *Inorg. Chem.*, 1978, **17**, 1501-1507.
23 P. M. Dias, D. L. A. Faria, V. R. L. Constantino, *Clays Clay Minerals*, 2005, **53**, 361-371.
24 T. Shiragami, K. Nabeshima, S. Nakashima, J. Matsumoto, S. Takagi, H. Inoue, M. Yasuda, *Bull. Chem. Soc. Jpn.*, 2005, **78**, 2251-2258.
25 T. Shiragami, K. Nabeshima, M. Yasuda, H. Inoue, *Chem. Lett.*, 2003, **2**, 148-149.
26 T. Shiragami, K. Nabeshima, J. Matsumoto, M. Yasuda, H. Inoue, *Chem. Lett.*, 2003, **6**, 484-485.
27 M. Ogawa, Y. Ide, T. Okada, *Chem. Asian J.*, 2010, **7**, 1980-1992.
28 S. Takagi, T. Shimada, Y. Ishida, T. Fujimura, D. Masui, H. Tachibana, M. Eguchi, H. Inoue, *Langmuir*, 2013, **29**, 2108-2119.
29 T. Tsukamoto, T. Shimada, S. Takagi, *J. Phys. Chem. A*, 2013, **117**, 7823-7832.
30 T. Tsukamoto, T. Shimada, S. Takagi, *J. Phys. Chem. C*, 2013, **117**, 2774-2779.
31 M. Sohmiya, M. Ogawa, *Microporous Mesoporous Mater.*, 2011, **142**, 363-370.
32 T. Egawa, H. Watanabe, T. Fujimura, Y. Ishida, M. Yamato, D. Masui, T. Shimada, H. Tachibana, H. Inoue, S. Takagi, *Langmuir*, 2011, **27**, 10722-10729.
33 T. Kuroda, K. Fujii, K. Sakoda, *J. Phys. Chem. C*, 2010, **114**, 983–989.
34 G. Villemure, C. Detellier, A. G. Szabo, *J. Am. Chem. Soc.*, 1986, **108**, 4658–4659.
35 G. Villemure, C. Detellier, A. G. Szabo, *Langmuir*, 1991, **7**, 1215-1221.
36 S. Takagi, M. Suzuki, T. Shiragami, H. Inoue, *J. Am. Chem. Soc.*, 1997, **119**, 8712-8713.
37 L. A. Lucia, T. Yui, R. Sasai, S. Takagi, K. Takagi, H. Yoshida, D. G. Whitten, H. Inoue, *J. Phys. Chem. B*, 2003, **107**, 3789-3797.
38 T. Shiragami, J. Matsumoto, H. Inoue, M. Yasuda, *J. Photochem. Photobiol. C: Photochem. Rev.*, 2005, **6**, 227-248.
39 T. Shiragami, Y. Shimizu, K. Hinoue, Y. Fueta, K. Nobuhara, I. Akazaki, M. Yasuda, *J. Photochem. Photobiol. A*: *Chem.*, 2003, **156**, 115-119.
40 H. Inoue, S. Funyu, Y. Shimada, S. Takagi, *Pure Appl. Chem.*, 2005, **77**, 1019-1033.
41 S. Funyu, T. Isobe, S. Takagi, D. A. Tryk, H. Inoue, *J. Am. Chem. Soc*., 2003, **125**, 5734-5740.
42 T. Shiragami, Y. Andou, Y. Hamasuna, F. Yamaguchi, K. Shima, M. Yasuda, *Bull. Chem. Soc. Jpn.*, 2002, **75**, 1577-1582.
43 N. J. Turro, J. C. Scaiano, V. Ramamurthy, *Principles of Molecular Photochemistry*, *An Introduction*, University Science Books, 1st edn., 2008.
44 T. Azumi, *J. Spectroscopic. Soc. Japan*, 1971, **20**, 309-319.
45 M. V. De Paoli, H. S. De Paoli, E. I. Borissevitch, C. A. Tedesco, *J. Alloys and Compounds*, 2002, **344**, 27-31.